



Towards Practical Design Rules for Quantum Communications and Quantum Imaging Devices

Neil J. Gunther¹, Giordano B. Beretta
Imaging Systems Laboratory
HP Laboratories Palo Alto
HPL-2005-129
July 8, 2005*

bifurcation,
interferometer,
quantum path
integral, quantum
imaging

Recent advances in quantum communications and imaging (QCI) technologies have led to a burgeoning market for commercial applications. These new market forces place an emphasis on engineering design rather than fundamental science. To guarantee correct device design, the quantum engineer needs to be removed from the minutia of the science. This can be accomplished through a set of abstract design rules analogous to those already employed in the VLSI chip industry. This paper is the first to propose such quantum design rules for the analysis of QCI devices, in general, and quantum imaging devices comprised of lens-based optics, in particular. We anticipate that these quantum design rules will also lead to significant cost reductions in the commercial production of quantum devices.

* Internal Accession Date Only

Approved for External Publication

¹Performance Dynamics, 4061 East Castro Valley Blvd., Castro Valley, California, USA

To be published in and presented at the Proceedings 5893 of Optics & Photonics: Quantum Communications and Quantum Imaging III, July 31- August 4, 2005, San Diego, CA

© Copyright 2005 Society of Photo-Optical Instrumentation Engineers

Towards Practical Design Rules for Quantum Communications and Quantum Imaging Devices

Neil J. Gunther^a and Giordano B. Beretta^b

^aPerformance Dynamics, 4061 East Castro Valley Blvd., Castro Valley, California, USA;

^bHP Laboratories, 1501 Page Mill Road, Palo Alto, California, USA

ABSTRACT

A common syndrome in much of the current quantum optics and quantum computing literature is the casual switching between classical concepts (e.g., geometric rays, electromagnetic waves) and quantum concepts (e.g., state vectors, projection operators). Such ambiguous language can confuse designers not well versed in the deeper subtleties of quantum mechanics, or worse, it can lead to a flawed analysis of new designs for quantum devices. To validate that a quantum device can be constructed with the expected characteristics and that its quantum effects are correctly interpreted, a set of unambiguous design rules would be useful. In this paper we enumerate such a set of easily applied quantum rules in the hope that they might facilitate clearer communication between researchers and system developers in the field. In part, we are motivated by recently reported interferometer results that have not only led to flawed claims about disproving fundamental quantum principles, but have elicited equally flawed counter arguments from supposedly knowledgeable respondents. After one hundred years of testing Einstein's photon, it is alarming that such widespread confusion still persists. Our proposed quantum design rules are presented in a practical diagrammatic style, demonstrating their effectiveness by analyzing several interferometers that have appeared in the recent literature. Application to other quantum devices e.g., quantum ghost imaging, are also discussed. We stress that these rules are entirely quantum in prescription, being particularly appropriate for single-photon devices. Classical optics concepts e.g., refractive index, are not required since they are subsumed by our quantum rules.

Keywords: bifurcation, interferometer, quantum path integral, quantum imaging

1. INTRODUCTION

All these fifty years of conscious brooding have brought me no nearer to the answer to the question, 'What are light quanta?' Nowadays every rascal thinks he knows, but he is mistaken.

—Einstein to Besso (1951)

In this centennial year since Einstein's radical hypothesis that Maxwell's classical electromagnetic fields should (somehow) be regarded as having a quantized structure in order to correctly account for their interaction with matter (e.g., photoelectric phenomena¹), and more than fifty years after his comment to Besso, we are still in the position that although we have uncovered ever more exotic properties of light than those considered by Einstein, we have not achieved a deeper understanding of the photon. On the other hand, it is clear that today we are in possession of the correct quantum rules for determining how the photon interacts with matter—up to and including the most recent novel cases (e.g., quantum cryptoFAXing^{2,3} and quantum interrogation⁴⁻⁶).

N.J.G.: www.perfdynamics.com/emailform.html (For correspondence)

G.B.B.: www.hpl.hp.com/personal/Giordano_Beretta/ (*In memoriam, Yoko Nonaka*)

Copyright © 2005 Society of Photo-Optical instrumentation Engineers. This paper will be published in the Proceedings 5893 of Optics & Photonics: Quantum Communications and Quantum Imaging III, San Diego, Jul 31–Aug 4, 2005 and is made available as an electronic preprint with permission of SPIE. One print or electronic copy may be made for personal use only. Systematic or multiple reproduction, distribution to multiple locations via electronic or other means, duplication of any material in this paper for a fee or commercial purposes, or modification of the content of the paper are prohibited.

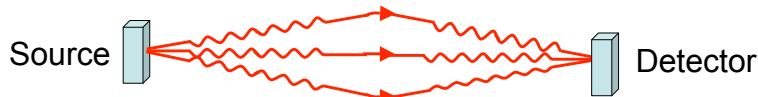


Figure 1. Three possible photon paths between a monochromatic source and a detector.

This situation seems not yet to have been fully acknowledged, as evidenced in the modern quantum-optics literature which can be viewed as falling into two broad categories: (i) quantum communications where the tendency is to emphasize the *particle* nature of photon by expressing its interactions with matter using an information-theoretic state-space^{7,8} or discrete-valued logic gates,⁹⁻¹¹ and (ii) quantum imaging where the tendency is to emphasize the *wave* nature of the photon through the use of Maxwellian field approximations.^{3,12}

In this paper, we attempt to remove that historical dichotomy by presenting a relatively simple set of quantum mechanical (QM) rules which are based neither on the particle nor the wave concept. These rules are aimed at the quantum-device engineer rather than the quantum physicist, per se. Our inspiration stems in part from Feynman’s Mautner Memorial Lectures¹³ on quantum electrodynamics (QED) where he begins by demonstrating that all of classical optics (and later all interactions of light with matter) can be understood and calculated entirely in terms of a set of simple arithmetic rules. Those seemingly benign rules are in fact a pictorial distillation of Feynman’s earlier *Quantum Path Integral* (QPI) formulation of quantum mechanics^{14,15} where the *physical* photon is represented by an infinite set of paths (quantum amplitudes) between source and detector. As far as we are aware, the idea of deriving the well-known results of classical optics from a purely quantum mechanical standpoint (with no more effort than vector addition) seems to be unique to Feynman and, with the exception of some novel pedagogic applications,¹⁶ appears to be largely unknown to the broader optics community.

The physical photon is only known to us as a consequence of a measurement process e.g., at a detector. What happens between emission and detection remains inscrutable. However, the measurement outcome can be correctly predicted by treating the transition between emission and detection as a multiplicity of possible paths that a physical photon could take (Fig. 1). These paths are to be regarded as sample paths in the stochastic sense. All paths between emission and detection are equally likely, but they contribute differently to the final probability which is the number that is compared with measurement at the detector. These are the QPI paths. Because of the multitude of QPI paths they can appear visually richer than other QM representations, and there is the temptation to incorrectly interpret them as offering a deeper philosophical significance. We scrupulously avoid being labeled one of Einstein’s rascals by not trying to promote the QPI as offering any deeper insight into the true nature of the physical photon than any other QM representation. We shall endeavor to shepherd the reader away from this potential pitfall throughout the subsequent discussion.

Drawing a multitude of QPI paths literally can cause visual clutter. If we were to draw the multiplicity of possible QPI paths as in Fig. 1, for example, the subsequent figures would become illegible. To minimize that problem, only significant QPI paths from the multitude are included in the diagrams. This also avoids the other mistake of drawing just a single path corresponding to the classical Fermat path.

The authors’ experience with VLSI design¹⁷ has made us aware of the importance of having correct design rules. Design rules provide an abstraction of physical reality so that when one makes the transition from pure physics to a commercial technology, one does not need to understand all of the underlying physical details. We have now reached that point with quantum communications and imaging devices. We shall emphasize the visual form of the quantum design rules because a visual representation offers one of the best cognitive impedance matches. Ultimately, we would like to see these rules embedded in automated design tools.⁸ Our design rules will be applied to several kinds of quantum devices, including those that explicitly use optics (e.g., lenses, apertures).^{3,18}

This paper is organized as follows. Sect. 2 presents the mathematical underpinnings of the QPI. Sect. 3 defines a set of operational design rules for analyzing quantum devices based on the mathematical properties outlined in Sect. 2. In Sect. 4 we apply these quantum rules to both classical optics and some well-known

quantum devices. In Sect. 5 we analyze a more complex quantum imaging device for which the conventional analysis¹⁹ leads to an erroneous conclusion. We demonstrate how our quantum design rules can be applied to reveal the source of the error. In Sect. 6 we briefly point out how the QPI formalism can be extended to include relativistic effects. Sect. 7 summarizes the main points of this paper and outlines future research directions for applying QPI analysis to quantum imaging and communication devices.

2. QUANTUM PATH INTEGRAL

In this section we briefly introduce some basic mathematical aspects of the quantum path integral (QPI) which will then be used to develop a more diagrammatic form of analysis in subsequent sections of this paper. Derivations and proofs can be found in the source literature and tutorials.^{14, 15, 20-23} The QPI is both a formal mathematical construction and a highly visual representation.

Definition 1 (Propagator): Every path $x(t)$, starting at a source point (x_s, t_s) and ending at a detector located at the point (x_d, t_d) in space and time (Fig. 1), receives a weight proportional to:

$$e^{iS[x(t)]/\hbar} \tag{1}$$

where the phase is represented by the classical action*

$$S[x(t)] = \int_{t_s}^{t_d} L dt, \tag{2}$$

i.e., the time-integral of the Lagrangian. ■

The Lagrangian is defined in terms of the kinetic energy $T(\dot{x})$ and the potential energy $V(x)$ as:

$$L = T(\dot{x}) - V(x), \tag{3}$$

for a Newtonian point-particle located at position x at time t and moving with velocity $\dot{x} = dx/dt$. It is important to note that the phase $S[x(t)]$ in eqn.(1) makes an explicit connection between classical mechanics and QM. In the examples we shall consider, the photon is treated as a free particle (i.e., $V(x) = 0$).

Definition 2 (Summation): The non-relativistic quantum propagator for a photon to go from source (s) to detector (d) is defined by the summation over all possible individual paths weighted according to eqn.(1):

$$G(x_d, t_d | x_s, t_s) = \mathcal{N} \sum_{\Gamma} e^{iS[x(t)]/\hbar} \tag{4}$$

where \mathcal{N} is a normalization constant, and Γ means all paths connecting (x_s, t_s) and (x_d, t_d) . In the continuum limit eqn.(4) can be written as a functional integral:

$$G(x_d, t_d | x_s, t_s) \equiv G(d|s) = \int_s^d e^{iS[x(t)]/\hbar} \mathcal{D}[x(t)]. \tag{5}$$

with the appropriate choice of integration measure. Hence the name quantum path integral[†]. ■

For a free massive particle the Lagrangian in eqn.(3) becomes $L = T(\dot{x}) = \frac{1}{2}m\dot{x}^2$, and the associated integration measure is:

$$\int \mathcal{D}[x(t)] = \lim_{N \rightarrow \infty} \left(\frac{m}{2\pi i\hbar(t/N)} \right)^{N/2} \prod_{i=1}^{N-1} \int dx_i \tag{6}$$

*The constant $\hbar = h/2\pi$ (where h is Planck's constant) is also known as Dirac's constant. The classical action $S[x(t)]$ and \hbar have the same physical dimensions, so the phase in eqn.(1) is dimensionless.

[†]The quantum path integral should not be confused with the more elementary *line* integral $\int_a^b \mathbf{F} \cdot ds$ of a vector-valued function \mathbf{F} along a curved path \mathbf{s} from a to b .

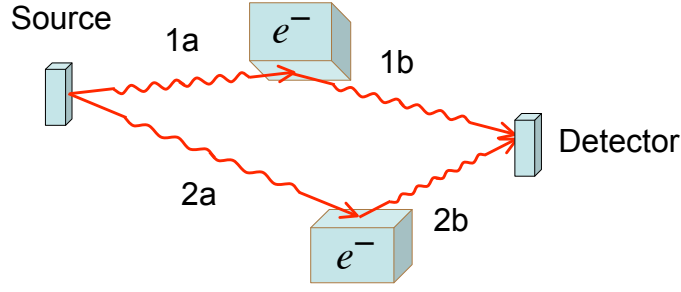


Figure 2. Two photon paths (1 and 2) between a source and a detector each of which undergoes an interaction with matter (i.e., with the electrons in it) as represented by the sub-paths (1a, 1b) and (2a, 2b). Since the photon is absorbed and reemitted with each interaction, they are not the same photons.

and the propagator to move from the origin to a point (x, t) is given by¹⁵ (Appendix A):

$$G(x, t|0, 0) = \sqrt{\frac{m}{2\pi i\hbar t}} \exp\left(i\frac{mx^2}{2\hbar t}\right) \quad (7)$$

Although the notion of integrating over an infinite collection of paths would seem intractable, in many cases the dominant contributions to eqns.(4) and (5) come from just a few paths (Fig. 1) because the remainder have highly oscillatory phases and thus their respective contributions cancel one another.¹⁵ We shall make use of this important fact throughout. Moreover, if $S[x(t)] \gg \hbar$ in eqn.(1) only one path contributes to the propagator viz., the path of a Newtonian particle which minimizes the action (2).²¹ For the photon, this stationary phase corresponds to the Fermat path.

Theorem 1 (Convolution): For any intermediate point x_i between x_s and x_d ,

$$G(x_d, t_d|x_s, t_s) = \int_{x_i} G(x_d, t_d|x_i, t_i) G(x_i, t_i|x_s, t_s) dx_i. \quad (8)$$

Equation (8) states that the propagator for any complete path $x(t)$ comprising two segments partitioned by (x_i, t_i) is determined by taking the product of the propagators for each of the path segments (Fig. 2). ■

The proof follows immediately from the additivity of the actions¹⁵ or the composition law for the QM evolution operator (see Sect. 2.2). Note that such products must be evaluated prior to the summation in eqn.(4) over all complete paths. The generalization of eqn.(8) to any number of multiple segments also holds and is the basis for eqn.(6).

2.1. Schrödinger Representation

Theorem 2 (Wave Function): The conventional QM wavefunction which solves the Schrödinger equation is defined in terms of the propagator eqn.(4) as:

$$\psi(d) = \int G(x_d, t_d|x_s, t_s) \psi(s) dx \quad (9)$$

This expression underscores the use of the term *propagator* for $G(d|s)$. Eqn.(9) takes the system from a state $\psi(s)$ to a state $\psi(d)$. ■

The proof follows from Theorem 1. From eqn.(9) it follows that $G(d|s)$ behaves like a Green's function. Defining

$$G_+(x_d, t_d|x_s, t_s) = \theta(t_d - t_s) G(x_d, t_d|x_s, t_s) \quad (10)$$

where $\theta(t)$ vanishes for $t < 0$ and is 1 otherwise ensures positive time causal solutions, then:

$$\left(-\frac{\hbar^2}{2m}\nabla^2 - i\hbar\partial_t\right)G_+ = \delta(t_d - t_s)\delta(x_d - x_s) \quad (11)$$

which establishes that the QPI is also a solution to the Schrödinger wave equation and therefore an equivalent representation of QM.

2.2. Dirac Representation

The QM time-evolution operator $U(t_d, t_s) = \exp[-iH(t_d - t_s)/\hbar]$, is expressed in terms of the Hamiltonian $H = p\dot{x} - L$, which is the Legendre transform of the Lagrangian in (2). The state $|\psi(t_d)\rangle$ of a quantum system at some final time t_d is determined by its initial state $|\psi(t_s)\rangle$ via $U(t_d, t_s)$:

$$|\psi(t_d)\rangle = U(t_d, t_s)|\psi(t_s)\rangle \quad (12)$$

The resulting wavefunction, expressed as the projection of the final state onto position basis states is given by:

$$\begin{aligned} \psi(x_d, t_d) &= \langle x_d|\psi(t_s)\rangle = \langle x_d|U(t_d, t_s)|\psi(t_s)\rangle \\ &= \int dx_s \langle x_d|x_s\rangle U(t_d, t_s)\langle x_s|\psi(t_s)\rangle \\ &= \int dx_s G(x_d, t_d|x_s, t_s)\psi(x_s, t_s) \end{aligned} \quad (13)$$

where we have introduced an orthonormal basis via the completeness relation $\int dx_s \langle x_s|x_s\rangle = 1$. Hence,

$$G(x_d, t_d|x_s, t_s) = \langle x_d|\exp^{-iH(t_d-t_s)/\hbar}|x_s\rangle \quad (14)$$

which establishes the connection between the QPI propagator and the time-evolution operator.

2.3. Density Matrix Representation

In the context of quantum computing, photonic qubits evolve reversibly according to eqn.(9) for $|\psi\rangle$, (11) and eqn.(12) since U can be replaced by U^\dagger . This assumes that the system can be completely isolated from its external environment. For a large number of identical non-interacting qubits, each in a state $|\psi\rangle$, is it often more convenient to describe the ensemble using a density operator:

$$\rho = |\psi\rangle\langle\psi| \quad (15)$$

The entropy of the ensemble can then be expressed in terms of eqn.(15) as:

$$S = -k \text{Tr}(\rho \ln \rho) \quad (16)$$

where k is Boltzmann's constant and Tr (*trace*) denotes the sum of the diagonal elements.

The connection between the statistical mechanics notion of reversibility²⁰ and the QPI comes from expressing eqn.(5) in terms of an imaginary time coordinate $t \rightarrow -it$ (Wick rotation) which takes eqn.(14) from complex-valued Hilbert space to a real-valued Euclidean space where:

$$\rho \equiv \int e^{-\beta S[x(t)]} \mathcal{D}x(t). \quad (17)$$

with $\beta = t/\hbar$. Hence, QM in imaginary time is logically equivalent to statistical mechanics at the inverse temperature $\beta = 1/kT$. An alternative normalization relates the partition function Z to the statistical density matrix $Z = \text{Tr}(\rho)$. In this Euclidean representation, the QPI sample paths become physical particles (e.g., a Boltzmann gas, atoms in crystal).

2.4. Photon Representation

Before proceeding to discuss the quantum design rules based on the QPI formalism, we should mention an often overlooked inconsistency in the treatment of the photon so far. Whether viewed classically or quantum mechanically, light is *relativistic*. In vacuuo, the photon has a velocity c and is *massless* (which accounts for the infinite range Coulomb force). However, the propagator defined in eqn.(7) is for a massive particle with a velocity $\dot{x} \ll c$. To see this, we note that the phase in the free particle propagator corresponds to the plane wave solution of the Schrödinger equation (11) (See Appendix B):

$$\psi(x, t) = e^{\frac{i}{\hbar}(px - Et)} \quad (18)$$

which follows from the associations:

$$p \rightarrow i\hbar\nabla \quad \text{and} \quad E \rightarrow \hbar\omega \quad (19)$$

On the other hand, the photon is more properly represented by the relativistic plane wave solution

$$A_\mu(x, t) = e^{i(px - kct)} = e^{ip_\mu p_\mu} \quad (20)$$

in 4-dimensional ($\mu = 0, 1, 2, 3$) space-time. It satisfies the Klein-Gordon wave equation¹⁴:

$$\left(\nabla^2 - \frac{1}{c^2} \partial_t^2 \right) A_\mu = 0 \quad (21)$$

for a massless, spin-1, vector boson, not the non-relativistic Schrödinger wave equation. The reconciliation between the quantum and the relativistic aspects of the photon leads to much more complex QED propagators¹⁴ than eqn.(7), and more complex than Einstein ultimately imagined²⁴ (See Sect. 6). On the other hand, for the non-relativistic energies we are considering here, full-blown QED would be overkill (but see Sect. 6). A more intermediate representation takes the photon paths to be the classical Fermat path together with neighboring QPI paths. It is in this sense that we are working in a semi-classical approximation for the photon (See Sect. 4.1 for more on this point).

In this section we have introduced the QPI formalism and shown that it is equivalent to other representations of QM used in the quantum communications and quantum imaging literature. In subsequent sections, we shall emphasize the visual aspects of the QPI paths as the basis for our quantum optical design rules.

3. QUANTUM DESIGN RULES

Hereafter, we focus on the photon as the quantum particle of interest, but before continuing let us recap the the implications of Sect. 2 for the design rules we are about enumerate.

The QPI formalism is mathematically rigorous but the physical implications are extremely odd. It tells us that the results of measuring a physical photon correspond to summing up every conceivable path that the photon could have taken between source and detector, then taking the absolute square of that sum. By this is meant not just a few paths like those shown in Fig. 1 or even a few hundred paths, but *all* possible paths. Prima facie this seems entirely unphysical, but it is part and parcel of the obscure nature of QM and reinforces Bohr's position.²⁵ As a counterpoint to this obscurity, however, the QPI does provide us with a clear visual representation that is neither particle nor wave based yet, by virtue of its association with the classical action, is not too far removed from our notion of a classical point particle.

Definition 3 (Quantum Optical Device): By quantum optical device we shall mean any apparatus that employs coherent or correlated photons (especially single photons or entangled photons) as part of its technology. Based on the QPI formalism of Sect. 2, the fundamental operational rules for these devices can now be stated.

Rule 1: The physical photon is a quantum entity. To avoid ascribing any deeper interpretation to the photon, we consider only the calculational rules for the QPI paths defined in Sect. 2.

Rule 2: Photons only interact with electrons (Fig. 2), not other photons. Such interactions are called *events*.

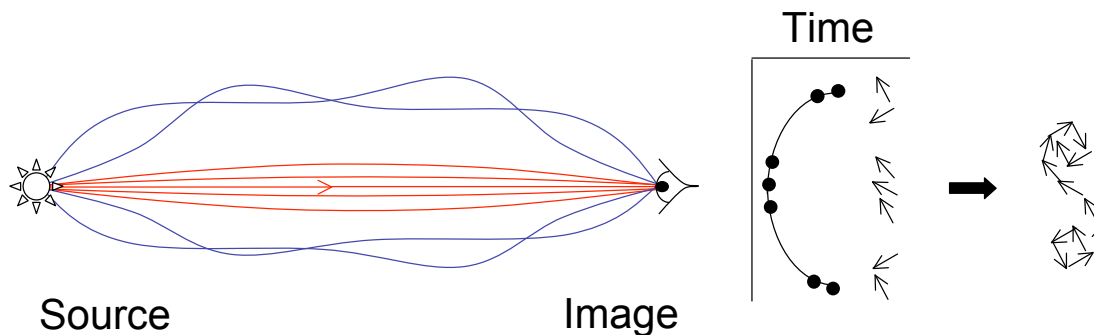


Figure 3. Sample QPI paths corresponding to emission of light from a standard source and imaged in the eye. As indicated by the angle of the arrows,¹³ paths that make long excursions away from the optical axis take a longer time to reach the image plane and have phases that cancel each other. The vector addition of a complete set of arrows (not shown) produces a crude Cornu spiral.

Rule 3: All matter contains electrons. Introducing any material into a quantum optical device introduces electrons which can affect the behavior of the photons in that device by virtue of events.

Rule 4: Between interaction events, the photon acts like a free particle (cf. Appendix A) following an arbitrary path. The difference between paths is determined by the corresponding phase function $S[x(t)]$ in eqn.(2) for that path. The final interaction event is detection.

Rule 5: A photon that undergoes an intermediate interaction event (i.e., other than detection) starts a new QPI path segment (as a different photon) until the next event. The detailed physics of the interaction between photons and electrons (which is the domain of QED) is not described in this approximation. See Sect. 6.

Rule 6: The contribution of successive path segments within a complete QPI path between source and detector is determined by taking the *product* of the propagators belonging to each segment. This follows from eqn.(8). These products must be evaluated prior to performing any summation (superposition) of complete QPI paths.

Rule 7: All possible photon paths must be considered when computing the outcome for a physical photon. In practice this means scrutinizing for the most likely paths that contribute to the *sum* in eqn.(4). In certain cases (e.g., Sects. 4.3 and 4.5) the number of contributing QPI paths can be very few. Photon paths that take nearly equal times to reach the detector will have phases that tend to reinforce each other. Otherwise, paths will make reduced contributions as they tend to cancel each other. See Sect. 4.1 for more details.

Rule 8: The only quantity that can be compared with the result of a physical measurement is the absolute square of the QPI propagator:

$$Pr_{\gamma}(d) = \overline{G(d|s)} G(d|s) \equiv |G(d|s)|^2 \quad (22)$$

which is the probability of detecting a physical photon at (x_d, t_d) .

4. APPLYING DESIGN RULES

To establish the credibility of the quantum design rules developed in Sect. 3 we apply them to several well-known examples.

4.1. Convergent Lens

Since the QPI description of how a convergent lens operates will be central to our discussion in Sect. 5, we begin by applying our design rules to a lens in a manner similar to that presented by Feynman¹³—which emphasizes the visual rather the calculation aspects of the QPI.

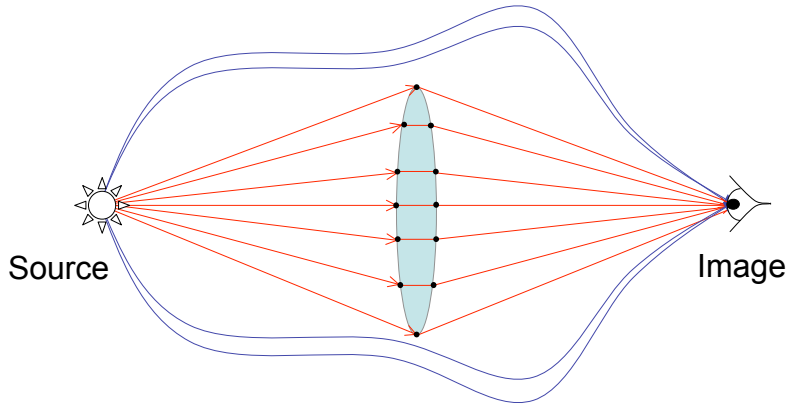


Figure 4. A highly idealized representation of a convergent lens in the QPI representation. QPI paths that pass through the lens reach the eye at the same time because those paths near the center of the lens must traverse a proportionately thicker amount of glass at a slower speed than paths near the periphery of the lens. Similar to Fig. 3, paths outside the area of the lens still reach the eye but arrive with different phases that tend to cancel each other.

Consider a standard source of light as seen by the observer depicted in Fig. 3. Classical optics tells us that such light travels in straight lines (or geodesics) and can therefore be represented by geometric rays. The QPI view, on the other hand, represents light as an infinite multitude of possible paths (not just a straight line) between the source and the image. Not all paths have the same length between source and detector, and we know from Sect. 2.4 that the physical photon has a constant speed c . Therefore, in order to arrive at the detector at a given time, photons that travel longer distances must be emitted earlier than those that travel a shorter distance. The exact times of emission cannot be known because of Heisenberg’s uncertainty principle. Since we know the energy of a monochromatic photon from eqn.(19) precisely, we cannot know the exact time of emission; we can only know a time interval.

Within that interval there will be a multiplicity of emissions producing a *tube of paths* shown in red in Fig. 3. Each of these QPI paths has associated with it a weight given by eqn.(1) where the distinction between paths is expressed entirely in the phase $S[x(t)]/\hbar$ of eqn.(2). More pictorially, Feynman¹³ associates the phase of each path with the hand of an imaginary stopwatch[‡] shown as the small arrows in Fig. 3. The multiplicity of emission times corresponds to the angle of Feynman’s arrows. Also shown in Fig. 3 is the corresponding Cornu spiral²⁶ formed by vector addition of the arrows. Those arrows corresponding to the tube of QPI paths have very similar angles and therefore produce the major contribution to the path integral. In this sense, the tube of QPI paths reinforce one another. The arrows are, of course, an oblique reference to the fact that a QPI path is formally a complex vector in Hilbert space. The angle of each arrow at the image plane corresponds to the value of its phase at emission. Each arrow is then added vectorially (Rule 7) and the absolute square of the result is compared with measurement^{13,16} (Rule 8). Feynman goes on to analyze internal reflection, mirrors, and lenses in this way. Rather than repeat all that here, the reader is encouraged to peruse Feynman’s book.¹³

The uncertainty of the emission time which leads to the existence of the tube of QPI paths is a fundamental physical property, unrelated to the noise in an observation. This measurement error can be made as small as desired by using standard techniques such as cooling the emitter, the detector, and other critical elements in the apparatus, as well as measuring entangled photon coincidence counts.

The operation of a lens, from the QPI standpoint, builds on the concepts in Fig. 3. Ideally, the lens arrangement in Fig. 4 has infinite diameter. The lens has the effect of slowing down those QPI paths that pass through it because the photon interacts (through scattering, absorption, reemission) with electrons belonging to the atoms

[‡]The analogy is false in the sense that a stopwatch implies QPI paths with amplitudes $\exp(+i\omega t)$, whereas plane wave solutions for a free photon imply $\exp(-i\omega t)$. The choice of sign has no impact on the outcome of calculations.

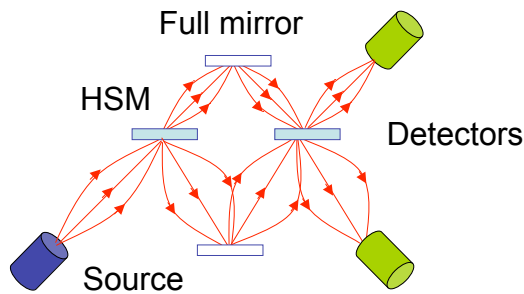


Figure 5. Photon paths in a Mach-Zehnder interferometer with half-silvered mirrors (HSM). The surviving QPI paths are drawn as a tube of paths around the Fermat path.

that comprise the glass (Rule 2). Of course, similar interactions occur between photons and the electrons in the atoms of air (in an unevacuated device) but we shall ignore that detail here. Those QPI paths that pass through the center of the lens take slightly longer to reach the image plane than do those that pass near the perimeter of the lens. Therefore, all QPI paths that pass through the lens will take the same total time and have phases that additively reinforce at the image plane. All other QPI paths will tend to arrive with phases that cancel each other. In other words, the surviving QPI paths are *isochronous* paths. Notice that in this account we have not made use of conventional concepts such refractive index and Snell’s law.

In conventional optical analysis, the object undergoes a Fourier transform, and the image is formed by the inverse Fourier transform of the transformed object. In the QPI representation, the same effect arises from the fact that all QPI paths take the same time to reach the image plane. Essentially, if the total time for all paths is τ , and the time for a particular path to the lens is t_L , then the paths from the image to the lens are associated with weights $\exp(-i\omega t_L)$ and the sum over those paths corresponds to the Fourier transform. Conversely, the paths from the lens to the image plane are associated with weights $\exp(-i\omega(\tau - t_L))$, and the second term in the exponent gives rise to the inverse Fourier transform.

4.2. Mach-Zehnder Interferometer

The Mach-Zehnder interferometer (MZ) is comprised of a pair of birefringent crystals or half-silvered mirrors (HSM in Fig. 5) acting as beam splitters together with a full mirror in each arm.²⁶ This arrangement introduces multiple QPI path segments between the photon source and the detectors. Proper evaluation of this device therefore requires application of the convolution Rule 6.

Figure 5 is most commonly drawn as though each MZ segment is traversed by a single Fermat path of classical optics. From the QPI standpoint, however, this is only an approximation. As explained in Sect. 4.1, there must be a surviving tube of QPI paths in each segment. Moreover, the tube of possible photon sample paths is required for the correct quantum analysis, even when only a *single* physical photon (Fock state) is present in the MZ. This becomes important, for example, if a small aperture were to be placed in any MZ segment. It could significantly alter the phase cancellations in each QPI path and thereby produce a very different measurement. In Sect. 5.2 we consider a more detailed application of the MZ.

4.3. Pure Interference

As noted in Sect. 4.2, a formal calculation of pure interference effects in the MZ should take into account all possible QPI path segments in each arm of the MZ. However, for a Youngian double-slit interferometer (see Fig. 8) there is a legitimate short-cut. It is already well-known that interference fringes arise from the phase

difference δ due to the difference in path length between the two slits and the detector or a particular location on the screen. It turns out,²⁷ that it is sufficient to take as few as two QPI paths A_1 and A_2 defined as:

$$A_1 = a_r a_t e^{-i\omega t_1} \quad \text{and} \quad A_2 = a_t a_r e^{-i\omega t_2} \quad (23)$$

where we are writing the propagators in the photon representation of Sect. 2.4 with a_r and a_t the complex-valued amplitudes for reflection and transmission respectively at the second HSM in Fig. 5. From Rule 7, the path integral can be expressed simply as $G(d|s) = A_1 + A_2$. The probability $Pr_\gamma(d)$ for detecting photons is given by Rule 8:

$$\begin{aligned} Pr_\gamma(\delta) &= \overline{G(d|s_1)} G(d|s_2) \\ &= \overline{(A_1 + A_2)}(A_1 + A_2) \\ &= 2A_r A_t (1 + \cos \delta) \\ &= 4A_r A_t \cos^2\left(\frac{\delta}{2}\right) \end{aligned} \quad (24)$$

where $A_r = \overline{a_r} a_r$ and $A_t = \overline{a_t} a_t$ are the reflection and transmission *probabilities*, and $\delta = \omega(t_2 - t_1)$ is the phase difference between the two QPI paths at that location on the screen or that position of the detector.

Since this is an interference phenomenon, neighboring paths within the QPI tubes belonging respectively to A_1 and A_2 do not contribute at the screen. The half-angle formula in eqn.(25) conforms to the standard Maxwell wave theory result²⁶ for the intensity of the fringe pattern. Note that the result is the same but both the derivation and the interpretation are different. The derivation does not use Maxwell theory and the computed quantity is not an intensity but a probability: the probability of finding the physical photon at that location. Moreover, the multiplicity of QPI sample paths are still required to produce eqn.(25) even for the case of interference due to a *single* physical photon. This illuminates Dirac's comment "a single photon interferes with itself" to produce the observed fringes.²⁸ Once again, the QPI does not offer any deeper explanation of the physical photon, it merely confirms that a superposition of states must be considered in all QM measurements.

We can now draw an important distinction between *interference* and *interaction*. The observed fringes belonging to the interference pattern are a result of an interaction of photons with the electrons in the material that constitutes the image plane or detector i.e., a measurement process. By Rule 8, the probability associated with that measurement is given by the absolute square of the sum over QPI paths. Interference, on the other hand, arises from the sum over paths (superposition) of coherent photon propagators (23). See Sect. 5.3.

4.4. Diffractive Effects

Diffraction occurs due to interaction of photon paths with the geometry of the material aperture. According to Rule 3 the material aperture contains electrons and they influence the photon paths. In the QPI formalism the effect of an interaction event at the aperture can be understood by considering the photon paths from the source to the aperture, followed by the photon paths from the aperture to the detector or image plane. This is a manifestation of the QPI convolution Rule 6 based on Theorem 1.

Writing a square aperture function $F(y) = \frac{1}{2}[sgn(y + \frac{1}{2}) - sgn(y - \frac{1}{2})]$ and applying eqn.(9) produces:

$$\begin{aligned} \psi(k) &= \int_{-\infty}^{\infty} F(y) \exp(iky) \exp(ik(x_0 + y)) dy \\ &= \exp(ikx_0) \frac{\sin(k)}{k} \end{aligned} \quad (26)$$

The first two factors in eqn.(26) reveal that the QPI acts like a Fourier transform on the rectangular function to produce the well-known *sinc* function²⁶ (cf. Sect. 4.1). Note that eqn.(26) is written in the momentum representation (Appendix C) The probability $Pr(d) = \overline{\psi} \psi$ produces a squared sinc function which corresponds to the classical wave theory intensity.²⁶ In a similar way it can be shown that a circular aperture produces the Airy disk.^{19,26} Diffraction can also modulate the pure interference pattern calculated in Sects. 4.3 and 5.1.

4.5. Entangled Interference

Entangled photon states (especially correlated biphotons) have been widely adopted in qubit encoding and imaging devices. Each of the preceding devices mentioned in this section have been studied using biphotons where the signal and idler are separated such that they are created collinear but with anti-parallel momentum at the parametric down conversion source (e.g., β -Barium Borate). The signal undergoes all the interactions in the device while the idler merely provides the coincidence tag.²⁹

An intriguing variant of this arrangement has been applied to quantum imaging.³ An object is placed between the biphoton source and a detector on the signal (idler) side. A convergent lens is inserted between the source and the object plane. The opposite side of the source is then scanned by either a single photon detector or a detector array.¹⁸ A ghost image appears by counting coincidence events between the two detectors. This effect has been analyzed using a semi-classical *advanced wave* model^{3, 12, 30-32} where the detector on the object side is thought of as being a source of standard light which illuminates the entire optical device with conventional geometric rays propagating backwards⁸.

Entangled interference requires that (Type I) biphotons are collinear with parallel momentum. We write the significant QPI sample paths as²⁷:

$$A_{11} = a_r a_t e^{-i(\omega_0+\omega)t_1} a_r a_t e^{-i(\omega_0-\omega)t_1} \quad (27)$$

$$A_{22} = a_r a_t e^{-i(\omega_0+\omega)t_2} a_r a_t e^{-i(\omega_0-\omega)t_2} \quad (28)$$

$$A_{12} = a_r a_t e^{-i(\omega_0+\omega)t_1} a_t a_r e^{-i(\omega_0-\omega)t_2} \quad (29)$$

$$A_{21} = a_r a_t e^{-i(\omega_0+\omega)t_2} a_t a_r e^{-i(\omega_0-\omega)t_1} \quad (30)$$

where a U.V. pump photon (γ_p) produces a pair of correlated photons (γ_s and γ_i) with energies differing by 2ω about a common frequency $\omega_0 = \omega/2$ such that both energy ($\omega_s = \omega_0 - \omega$, $\omega_i = \omega_0 + \omega$) and momentum ($k_s = k_0 - k$, $k_i = k_0 + k$) are conserved²⁷:

$$\hbar\omega_p = \hbar\omega_s + \hbar\omega_i \quad (31)$$

$$\hbar k_p = \hbar k_s + \hbar k_i \quad (32)$$

It is noteworthy that all four QPI paths in eqns.(27-30) look like an application of the convolution Rule 6 for two-path segments. A biphoton path starts at the source, undergoes an event, and reaches the detector. But the event in this case *is* the detector! In other words, each complete QPI path could be regarded as being composed of a path segment that goes from a source to a detector together with a simultaneous path segment that goes from detector to source as shown in Fig. 6. Eqns.(27) and (28) correspond to biphoton QPI paths in the same interferometer arm (Fig. 6a-b), while eqns.(29) and (30) correspond to biphoton QPI paths in opposite interferometer arms (Fig. 6c-d). These QPI loops carry overtones of the backward geometric rays of the advanced wave model, except that here they are true quantum paths. Fig. 7 shows how a topological rearrangement of the biphoton loop in Fig. 6(d) might be used to analyze quantum ghosting.³

Writing $\theta = \omega\Delta t$ and δ defined as before, the calculation of the coincident biphoton interference probability proceeds in the same way as Sect. 4.3:

$$\begin{aligned} Pr_{\gamma^2}(\delta) &= \overline{G(d|s_1)} G(d|s_2) \\ &= \overline{(A_{11} + A_{22} + A_{12} + A_{21})} (A_{11} + A_{22} + A_{12} + A_{21}) \\ &= 2A_r^2 A_t^2 [1 + 2(\cos\theta + \cos\delta)^2 - 2\cos^2\delta + \cos 2\delta] \\ &= 4A_r^2 A_t^2 (1 + \cos\delta)^2 \end{aligned} \quad (33)$$

where $\cos\theta \simeq 1$ for small θ . Eqn.(33) is the square of eqn.(24) resulting in narrower predicted fringes.²⁷

⁸Advanced wave solutions are part of the historical development of QED^{14, 33} (e.g., an electron moving backwards in time corresponds to its positron anti-particle) as well as other QM models.^{34, 35}

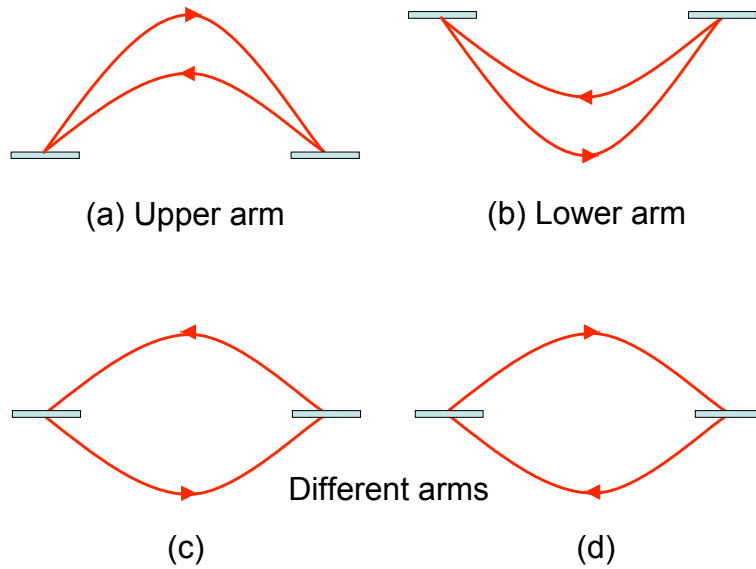


Figure 6. Possible QPI paths for entangled photon propagation in the two arms of a schematic MZ or Michelson interferometer corresponding to eqns.(27–30). Both correlated photons may traverse each arm together (a) and (b) or they may traverse different arms individually (c) and (d). Each of the biphotons has a separate propagator which is multiplied in the path integral due to their intrinsic correlation. But this is logically equivalent to Rule 6, so one of the biphotons can be considered to travel “backwards” from the detector to the source.

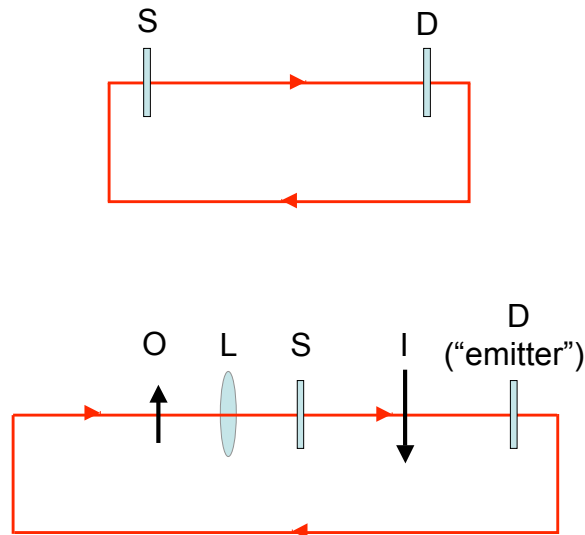


Figure 7. The upper diagram is a topological equivalent rearrangement of the biphoton loop in Fig. 6(d). If an object O and a convergent lens L are placed to the left of the biphoton source S and the detector at D is also regarded as an “emitter”, the arrangement bares a striking resemblance to the advanced wave interpretation of quantum ghosting.^{3,30,31}

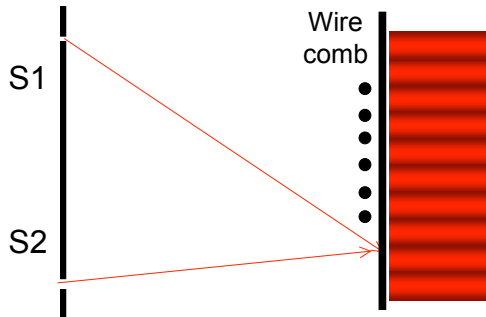


Figure 8. YAW interferometer showing the visible interference fringes ($\lambda = 650$ nm) produced on an opaque screen. Six fine wires are positioned exactly where intensity minima occur at the center of the apodized Airy disk (not shown). See Sect. 4.4

5. CASE STUDY

We turn now to a more detailed application of the design rules in Sect. 3. In particular, we consider a more complex quantum imaging device, the recent analysis¹⁹ of which has led to erroneous conclusions about the wave-particle nature of the photon. As a measure of the importance of having the correct tools, we demonstrate how our quantum design rules reveal the error in that analysis.

Bohr’s *Principle of Complementarity*²⁵ states that we cannot measure both the photon’s exact path to the screen ($K = 1$) and its wave character which produces interference fringes with visibility $V = 1$. In a novel variation of the classical Young interferometer,^{19, 36–40} the usual image plane where the fringes are observed is replaced with a convergent lens (like a camera) which focuses two image spots ($K = 1$) onto a different image plane behind the lens in the presence of interference ($V = 1$). This result implies that $V^2 + K^2 = 2$ in contradiction to Bohr’s principle.

Given the durability of quantum theory over the past 85 years, and the number of recent experimental results^{7, 41–43} which support a more subtle variant of Bohr’s principle viz., $V^2 + K^2 \leq 1$, we can safely assume that the claim about contradicting complementarity is flawed. One has to be careful in measuring V and K because of the robustness of V in the presence of dominant path information. For example, even when $K = 0.9980$, visibilities on the order of 4–5% have been observed.⁴¹ More significant for our purposes is determining where the error in the analysis lies. For that, we apply the design rules of Sect. 3.

5.1. YAW Interferometer

So-called *delayed choice* interferometers^{44–46} have been proposed with the idea of deciding how to measure the photon after it leaves the pinholes, either by looking at the pinholes with telescopes to see from which pinhole the photon was emitted ($K = 1$) or by inserting a screen and viewing the interference fringes ($V = 1$). A more recent variant¹⁹ of Wheeler’s thought apparatus entails two modifications: a wire comb and a convergent lens. An opaque screen is used to image the interference fringes and six fine wires (Fig. 8) are placed where the dark fringes appear. The opaque screen is then replaced with a convergent lens positioned behind the wire comb. Two photon detectors play the role of Wheeler’s telescopes⁴⁴).

We shall refer to this modified apparatus as the Young-Afshar-Wheeler (YAW) interferometer. The measurement process in the YAW proceeds in two stages:

1. One pinhole source (e.g., S_1 in Fig. 9) is closed. The single incoherent source (S_2) means there is no interference, and the wire comb therefore scatters approximately 6% of the total flux.
2. Next, both pinholes are opened to produce two coherent sources (Fig. 10). No light scatters off the wires in the presence of interference ($V = 1$). However, the two distinct image spots focused by the lens are also recorded at the detectors ($K = 1$). Hence, it appears that $V^2 + K^2 = 2$.

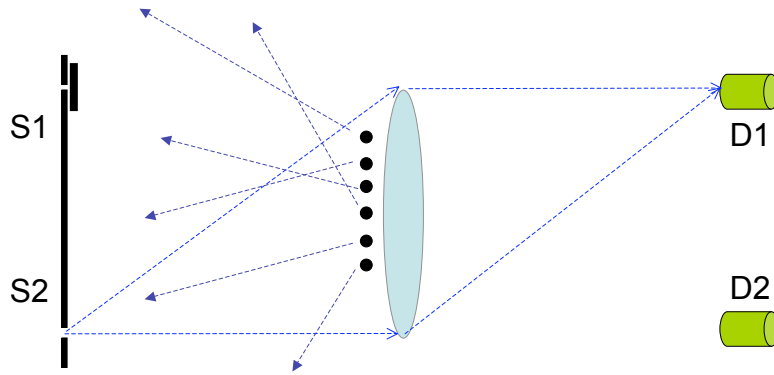


Figure 9. The screen in Fig. 8 is replaced by a convergent lens positioned behind the wire comb. If only one YAW pinhole is open (e.g., S_2) approximately 6% of the total photon flux is lost due to scattering off the wires. The source and detector separations are shown in one-to-one proportion for visual simplicity. The actual separations are $S_1-S_2 = 2$ mm, $D_1-D_2 = 0.6$ mm, using a lens of focal length 1000 mm and diameter 30 mm, positioned 4 m from the source plane with a total optical path length of 5 m.¹⁹

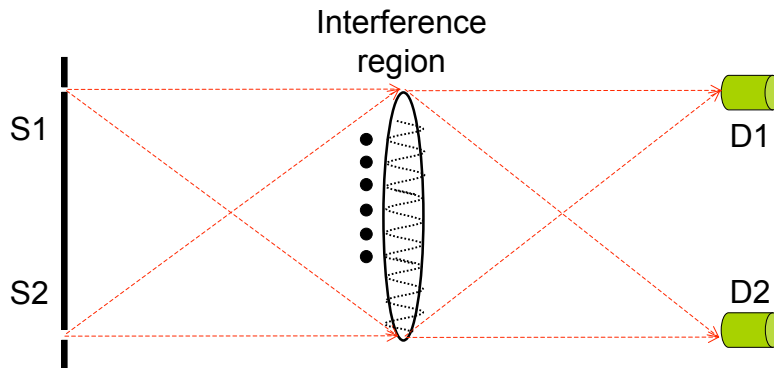


Figure 10. With both pinholes open, coherent light undergoes the usual interference in the region of the lens. Since the lens is transparent, no fringes are observed but the back scattering of Fig. 9 is also diminished. Since photons also reach the detectors D_1 and D_2 the source pinholes can also be imaged. The source and detector separations are shown in one-to-one proportion for visual simplicity.

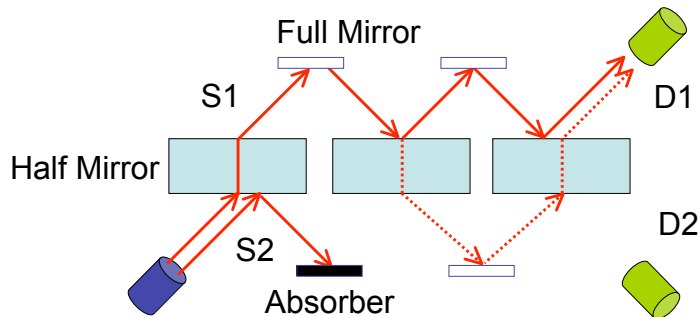


Figure 11. Tandem MZ interferometer of Unruh.³⁷ A conventional MZ interferometer is shown in Fig. 5

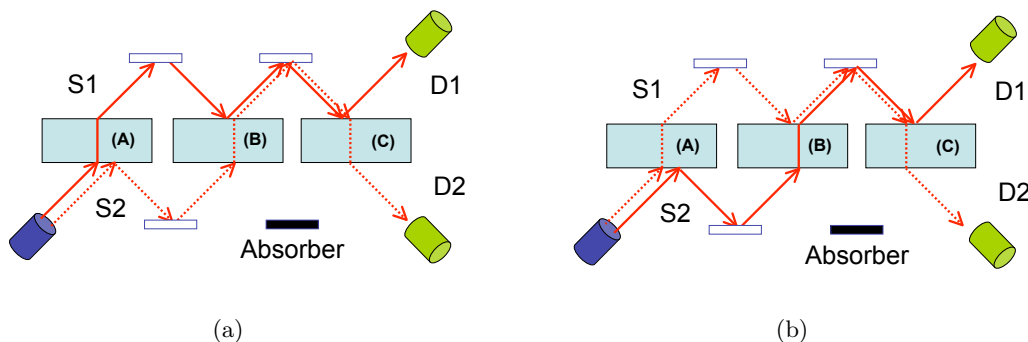


Figure 12. With interference present in the upper channel of the UMZ, the exact path the photon takes between source and detector cannot be determined. Detector D_2 always sees “dotted” photons irrespective of whether those photons emanated from source S_1 12(a) or S_2 12(b).

5.2. UMZ Counterexample

The tandem MZ interferometer in Fig. 11 proposed by Unruh³⁷ can be used to verify that path information must be lost in the presence of interference. We shall refer to this apparatus as the Unruh-Mach-Zehnder (UMZ) interferometer. Fig. 11 is the logical equivalent of step 1 in the YAW measurement procedure. The half-silvered mirror (HSM) at position (A) simply creates twin coherent photon sources. In this configuration, only photons on path S_1 can trigger detector D_1 . Similarly, for S_2 and D_2 . Hence, the photon’s path can be known and therefore, $K = 1$. No interference is present in Fig. 11.

Referring now to Fig. 12, the absorber between HSM (A) and (B) is repositioned between HSM (B) and (C), and replaced by a full mirror adjusted to produce interference at HSM (B). Constructive interference occurs in the upper channel and destructive interference in lower channel. This arrangement is logically equivalent of step 2 in the YAW procedure where the absorber represents the wire comb. The absorber provides a null measurement of complete interference ($V = 1$). For example, D_2 always sees a “dotted” photon coming from either S_1 or S_2 . This ambiguity is tantamount to destroying path information ($K \neq 1$).

Afshar dismisses Unruh’s analysis on the grounds that UMZ is not a faithful representation of YAW.³⁹ Subsequently, we show that Afshar is indeed vindicated on that particular point; YAW physics is subtly different, although Unruh’s argument is logically correct. Moreover, the UMZ analysis forces Afshar into the weaker position of claiming that we must use his special (more confounded) YAW interferometer in order to observe what is otherwise supposed to be a universal quantum effect.

Fig. 13 shows the mapping between the UMZ and YAW interferometers. The chief difference is that UMZ

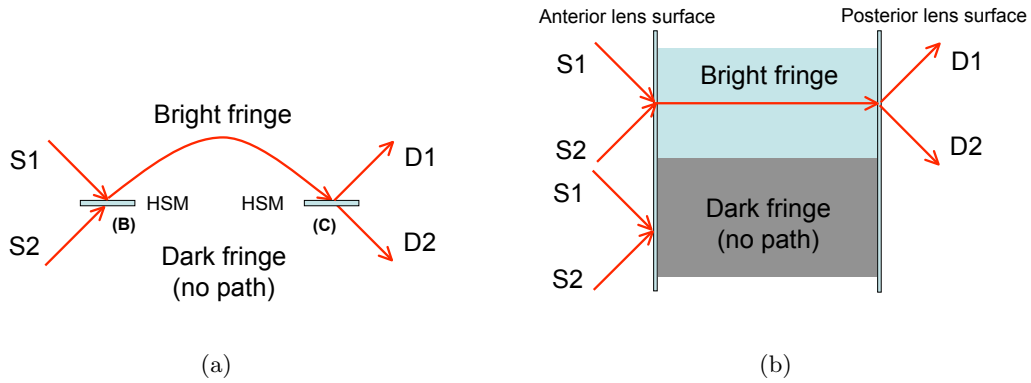


Figure 13. Minimal schematic form 13(a) of the UMZ interferometer in Figs. 11 and 12 mapped into a pseudo-lens form 13(b) of the same configuration.

involves birefringent beam splitters whereas the lens in YAW has a single index of refraction. How are we to resolve this paradox?

5.3. Coherent Bifurcation

The quantum path integral analysis of a convergent lens in Sect. 4.1 showed that the important QPI sample paths are *isochronous*, meaning that the significant contributions come from those QPI paths that take the same time to go from the light source to the image spot. All other QPI paths cancel at the image plane.¹³ This is the basis of the classical concept of *refraction* in the geometric ray approximation. Unlike the analysis of the UMZ in Sect. 5.2, it is not possible to have classical geometric rays going from source S_1 to the image spot at detector D_1 (and similarly for $S_2 \rightarrow D_2$) because of refraction. The one exception to this statement involves those rays which pass through the optical axis (OA) of the lens as depicted in Fig. 14.

A QPI path from S_1 , for example, has a 50/50 chance of proceeding to either detector D_1 or D_2 in the same elapsed time because these alternative legs have the same length[¶]. However, at other locations on the lens, above and below the OA, the legs have different lengths (unlike the UMZ in Fig. 13), and therefore neighboring paths along the route $S_1 \rightarrow D_1$ (or $S_2 \rightarrow D_2$) will not tend to cancel each other at the image plane.

That said, we pause to note that the above conventional refractive analysis holds for standard *incoherent* light sources, whereas the YAW interferometer involves twin *coherent* sources, so the analysis changes completely.⁴⁰ Now, we must take into account other quantum effects, which we do by applying our QPI rules of Sect. 3.

We consider the variety of ways QPI paths can reinforce each other like the tube of paths described in Fig. 3 and Sect. 4.1. Clearly, coherent QPI paths passing near the center of the lens in Fig. 14 can reach either detector in the same time (just as they would for twin incoherent sources). In addition, however, coherent paths from S_1 and S_2 reaching a point in the lens where there is *maximal* phase coherence (Fig. 15) will reinforce each other rather than cancel when they reach detector D_1 (Rule 7). Those QPI paths that reach the lens with *minimal* phase coherence will cancel and not be transmitted to the image plane. Those QPI paths that arrive at points on the lens which are intermediate between these two phase extrema will only reinforce each other partially and thereby be refracted in the same way as for incoherent light.

We caution the reader that the QPI paths from S_1 and S_2 in Fig. 15 cannot “interact” at the anterior surface of the lens (or anywhere else in the lens) because Rule 2 excludes that possibility. Rather, the contribution from

[¶]Logically, this would be sufficient to invalidate the conclusion regarding a violation of complementarity. A possible rejoinder might be that the effect represents only a very small contribution to the overall photon flux reaching the detectors. In the actual YAW device, however, the apodized Airy disk has its maximal fringe at the center of the lens.

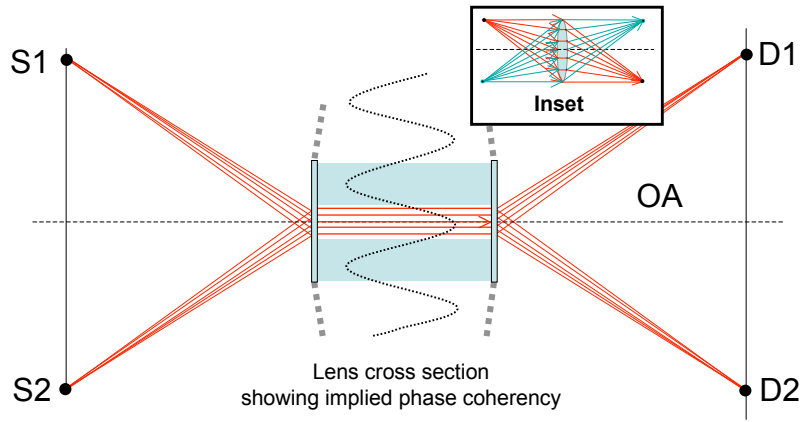


Figure 14. QPI paths showing how photons passing through the center of the lens will reinforce and undergo bifurcation to reach either detector. The source and detector separations are shown in one-to-one proportion for visual simplicity.

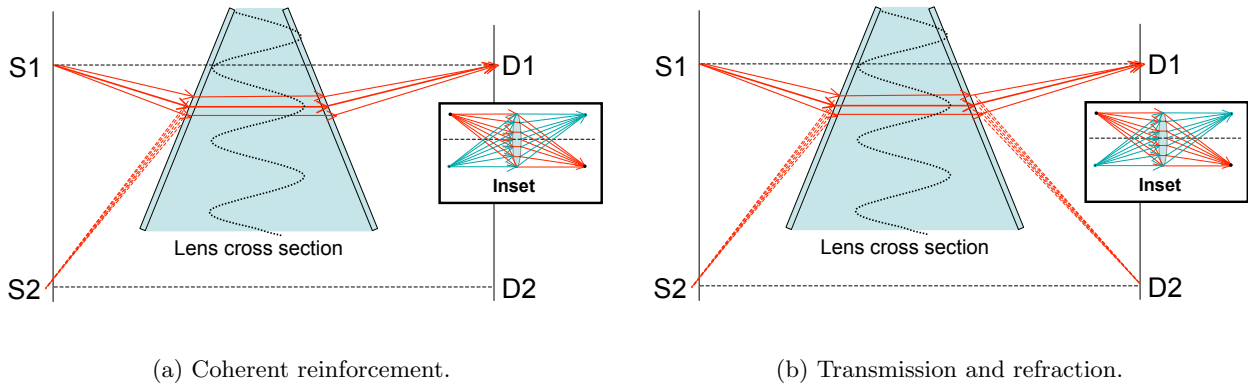


Figure 15. A set of QPI paths passing through a prismatic section of the convergent lens in Fig. 10 (inset) showing how bifurcation, similar to that in Fig. 14, occurs away from the optical axis (Fig. 15(a)). Depending on the degree of coherent reinforcement the QPI paths will arrive at either detector D_1 or D_2 (Fig. 15(b)). The source and detector separations are shown in one-to-one proportion for visual simplicity. Note that the QPI paths from S_1 and S_2 do not “interact” at the anterior surface of the lens because Rule 2 excludes this possibility.

reinforcing phases (i.e., the approximate alignment of Feynman’s arrows discussed in Sect. 4.1) is determined at the image plane, not at the lens.

In this way, we see that analyzing the non-classical QPI paths explains the YAW paradox,⁴⁰ and demonstrates (we trust) to the quantum design engineer the importance of playing by the rules in Sect. 3. Coherent bifurcation is responsible for each image spot receiving photons from both sources, presumably in equal proportions. The incorrect conclusion¹⁹ outlined in Sect. 5.1 rests on an inappropriate classical analysis using a geometric ray approximation. For twin *incoherent* light sources (e.g., headlights, stars) the phases belonging to paths from $S_1 \rightarrow D_1$ tend to cancel at detector D_1 . Only the isochronous paths $S_1 \rightarrow D_2$, and $S_2 \rightarrow D_1$ tend to reinforce each other. When the twin incoherent sources are replaced by *coherent* sources, non-classical optical effects arise. Phase-coherent paths can bifurcate inside the mono-refrangent lens.

Here, the term *bifurcation* is not meant to suggest that the physical photons splits in two. Rather, we mean that under these circumstances QPI paths can have two possible end-points at the image plane depending upon how the phase of a given path compares with the phase of its neighbors. This bifurcation of QPI paths is a property of the light, not the lens and it impacts the imaging process. We see also that the physics of quantum imaging in the YAW device is quite different from the birefringent beam splitters in the UMZ model.

The inclusion of all possible paths in the QPI would require that the lens have infinite diameter. In practice the YAW interferometer acts more like a long angled pipe (See Fig. 9 for the dimensions) in which the lens is fitted and is further restricted by an aperture to exclude manufacturing problems at the border of the lens. Consequently, some number of source photons are lost by absorption in the “walls” of the pipe and are not detected. Entangled biphoton coincidence counts could be used to offset these measurement losses.

As in a conventional lens, there are two image spots due to the symmetry of the QPI transform from the twin sources to the lens (Fourier transform) followed by the inverse Fourier transform of the interference region at the lens to the image plane (cf. Sect. 4.1). Since the lens images the interference region, not the YAW pinholes, the image spots will appear to have a concentric ring structure under ideal circumstances. This could constitute a test of the bifurcation model of the YAW paradox, but the effect would be subtle and is likely to be masked by such things as losses in the lens medium, diffraction at the pinholes, and Airy disks due to apodization. Alternatively, biphotons might provide a better means of demonstrate unequivocally that the image spots are comprised of photons from both sources.

6. RELATIVISTIC GENERALIZATIONS

The earliest controlled production of entangled photons was via positronium decay,⁴⁷ and there are current experimental tests of Bell’s theorem looking for relativistic effects in the apparatus.⁴⁸ These experiments are properly the domain of quantum electrodynamics (QED) and it seems fitting to briefly remark on the connection between the QPI formalism presented in this paper and its relativistic quantum generalization.

The path integral can be expressed in terms of field variables rather than particle coordinates. The QED counterpart of eqns.(2) and (3) involves the interaction field Lagrangian:

$$L_{int} = -e \int d^3x \bar{\psi} \gamma^\mu \psi A_\mu \tag{34}$$

where e is the electric charge, ψ and $\bar{\psi}$ are respectively the spinor solutions to the relativistic Dirac equation for spin $\frac{1}{2}$ fermions (i.e., electron and positron), and A_μ is the 4-vector potential of Sect. 2.4 representing the photon field. The γ^μ are the 4-dimensional generalization of the Pauli spin matrices required by antisymmetric fermion fields.

Equation (34) generates the diagrammatic rules for QED corresponding to those in Sect. 3. Since there are three fundamental fields: the electron, positron, and the photon, each vertex in Fig. 16 has degree three. In these 4-dimensional space-time diagrams, an upward-pointing arrow represents an electron and a downward-pointing arrow represents a positron (moving backwards in time). The photon has no arrow since it is its own anti-particle. In QED the photon plays a special role, it is the mediator of the electromagnetic force.

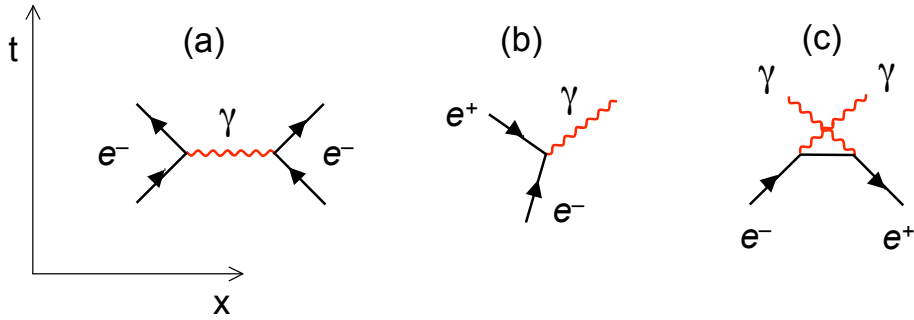


Figure 16. Relativistic space-time diagrams in quantum electrodynamics (QED) showing (a) electron-electron scattering via the exchange of a space-like virtual photon, (b) electron-positron annihilation to produce a light-like photon ($ds^2 = 0$), and (c) positronium decay producing entangled photons.⁴⁷

Although the non-relativistic design rules presented in Sect. 3 are likely sufficient for most current purposes, the QED generalizations may become more important in the future. In any event, the quantum designer needs to be *en garde* for the consequences of these more general effects.

7. CONCLUSION AND FUTURE WORK

In this paper we have taken a purely operational approach to the quantum phenomenon of the photon. Using the well-established quantum path integral (QPI) representation of quantum mechanics due to Feynman, we have demonstrated mathematically that this same quantum formalism can be applied consistently across an entire range of optical phenomena from classical optics to quantum imaging, treated at non-relativistic energies. We also emphasized that the QPI treatment is a semi-classical approximation for which the correct relativistic quantum generalization is already known viz., quantum electrodynamics. For many quantum devices QED analysis is overkill but the quantum designer needs to remain vigilant for such effects.

In Sect. 3 we encapsulated the mathematical characteristics of the QPI method in a set of quantum design rules and applied them to the analysis of several familiar quantum devices in Sect. 4. In Sect. 5 we used our quantum rules to analyze a more complex imaging device that has recently been claimed to produce *which-way* information in the presence of interference—in contradiction to the principle of complementarity. Applying our quantum rules, we were able to determine the source of the error in that analysis. The erroneous which-way analysis ultimately relies on classical Fermat paths instead of the more accurate QPI paths in the presence of interfering coherent sources. Under these circumstances light does not behave classically. The which-way information becomes lost via non-classical paths which can be regarded as bifurcating within the imaging lens itself: a property of the light, not the lens.

We have shown that the visual representation of the QPI is best done in the position representation, while calculations are best done in the momentum representation (see Appendices A and C). But even in the momentum representation the calculations involving optics can be rather formidable and are better solved programatically.^{49, 50} Ultimately, it would be advantageous to the quantum design engineer if these quantum rules could be incorporated into computer-aided design tools similar to those used by VLSI designers today.

As a further consequence of developing these quantum design rules, in Sect. 4.5 we have uncovered some heretofore unrecognized connections between entangled photonic qubits and loop structures in the quantum path integral. These paths with loops may offer deeper insight into the analysis of quantum ghost imaging as well as other entangled imaging phenomena. We intend to explore this further.

APPENDIX A. MASSIVE PARTICLE PROPAGATOR

From eqn.(2), the classical action for a free particle with mass m is:

$$S[x(t)] = \int_{t_s}^{t_d} \frac{1}{2} m \dot{x}^2 dt = \frac{m(x_d - x_s)^2}{2(t_d - t_s)} \quad (35)$$

These paths are straight lines in space and time since the velocity is constant. The QPI propagator can be calculated more easily in the momentum representation (cf. Feynman and Hibbs¹⁵ who use the position representation). Using the plane wave eigenkets:

$$H|p\rangle = \frac{p^2}{2m}|p\rangle \quad \text{and} \quad \langle x|p\rangle = \frac{1}{\sqrt{2\pi\hbar}} e^{ipx/\hbar} \quad (36)$$

the free particle propagator can be evaluated as:

$$\begin{aligned} G(d|s) &= \langle x_d | e^{-iH(t_d-t_s)/\hbar} | x_s \rangle \\ &= \int_{-\infty}^{\infty} \langle x_d | e^{-iH(t_d-t_s)/\hbar} | p \rangle \langle p | x_s \rangle dp \\ &= \int_{-\infty}^{\infty} e^{ipx_d/\hbar} e^{-i\frac{p^2}{2m\hbar}(t_d-t_s)} e^{-ipx_s/\hbar} \frac{dp}{2\pi\hbar} \\ &= \int_{-\infty}^{\infty} e^{-i\left(\frac{p^2}{2m\hbar}(t_d-t_s) + \frac{p}{\hbar}(x_d-x_s)\right)} \frac{dp}{2\pi\hbar} \\ &= \left(\frac{2\pi i\hbar(t_d-t_s)}{m}\right)^{-\frac{1}{2}} \exp\left(i\frac{m(x_d-x_s)^2}{2\hbar(t_d-t_s)}\right) \end{aligned} \quad (37)$$

in agreement with eqn.(7). The quantity $\sqrt{m/(2\pi\hbar t)}$ in the normalization prefactor has the physical dimensions of inverse length, while the factor $\sqrt{i} \equiv \sqrt{\exp(i\pi/2)}$ represents a rotation of the Hilbert vector by $\pi/4$.

APPENDIX B. PLANE WAVE SOLUTIONS

Writing the propagator in eqn.(7) as

$$G(x, t|0, 0) = C \exp\left(i\frac{mx^2}{2\hbar t}\right) \quad (38)$$

where C is a constant, and recognizing that the phase can be rewritten as:

$$i\frac{mx^2}{2\hbar t} = \frac{i}{\hbar} \int \frac{1}{2} m \dot{x}^2 dt = \frac{i}{\hbar} \int L dt \quad (39)$$

the following expansion of eqn.(38) ensues:

$$\begin{aligned} C e^{\frac{i}{\hbar} \int L dt} &= C e^{\frac{i}{\hbar} (\int p \dot{x} dt - \int H dt)} \\ &= C e^{\frac{i}{\hbar} (\int p dx - \int E dt)} \\ &= C e^{\frac{i}{\hbar} (px - Et)} \end{aligned} \quad (40)$$

which corresponds to the plane wave solution in eqn.(18).

APPENDIX C. DIFFRACTION OF A MASSIVE PARTICLE

The interested reader will find diffractive interference of a *massive* quantum particle (e.g., an electron) discussed in Feynman and Hibbs.¹⁵ Rather than solving for the case of a rectangular aperture, they consider a more mathematically tractable, but entirely artificial, ‘‘Gaussian’’ slit. For completeness, we solve the rectangular

case in the position representation for comparison with Sect. 4.4 which contains the result in the momentum representation. Applying eqn.(9) produces:

$$\begin{aligned}\psi(x) &= \int_{-\infty}^{-\infty} G(x+x_0, t|x_0+y, t-\tau) G(x_0+y, t-\tau|0, 0) dy \\ &= \int_{-\infty}^{-\infty} F(y) \left(\frac{2\pi i\hbar\sqrt{t(t-\tau)}}{m} \right)^{-1} \exp\left(i\frac{m(x-y)^2}{2\hbar t}\right) \exp\left(i\frac{m(x_0+y)^2}{2\hbar(t-\tau)}\right) dy\end{aligned}\quad (41)$$

where $F(y) = \frac{1}{2}[\text{sgn}(y + \frac{1}{2}) - \text{sgn}(y - \frac{1}{2})]$ represents a narrow rectangular aperture. The complete solution:

$$\begin{aligned}\psi(x) = \frac{1}{2\sqrt{t(2t-\tau)}} &\left((-1)^{\frac{1}{4}} \exp\left[\frac{im(x+x_0)^2}{\hbar(2t-\tau)}\right] \sqrt{m(2t^2-3t\tau+\tau^2)} \right. \\ &\left(\text{erfi}\left[\frac{(-1)^{\frac{1}{4}}\sqrt{m\pi(2t(x-x_0-1)+\tau-2x\tau)}}{2\sqrt{\hbar t(2t^2-3t\tau+\tau^2)}}\right] + \right. \\ &\left. \left. \text{erfi}\left[\frac{(-1)^{\frac{1}{4}}\sqrt{m\pi(2t(x-x_0+1)+\tau+2x\tau)}}{2\sqrt{\hbar t(2t^2-3t\tau+\tau^2)}}\right]\right] \right)\end{aligned}\quad (42)$$

hides the well-known physical result within the complex error functions. It is for this reason that the simpler momentum representation (Appendix A) of the QPI is preferred.

REFERENCES

1. A. Einstein, "Über einen die Erzeugung und Verwandlung des Lichtes betreffenden heuristischen Gesichtspunkt," *Annalen der Physik* **17**, pp. 132–148, 1905. (The seminal but disdained paper which proposed that all radiation comprises discrete quanta ultimately named "photons" in 1926 by G. N.Lewis.)
2. A. V. Sergienko, Y. Shih, T. B. Pittman, D. V. Strekalov, and D. N. Klyshko, "Two-photon geometric optical imaging and quantum cryptofax," in *Atomic and Quantum Optics: High-Precision Measurements*, S. N. Bagayev and A. S. Chirkin, eds., *Proc. SPIE Int. Soc. Opt. Eng.* **2799**, pp. 164–171, SPIE, (St. Petersburg, Russia), 1996.
3. M. D'Angelo and Y. Shih, "Quantum imaging," *Laser Physics* **15**, 2005.
4. G. J. Pryde, J. L. O'Brien, A. G. White, S. D. Bartlett, and T. C. Ralph, "Measuring a photonic qubit without destroying it," *Physical Review Letters* **92**(19), p. 190402, 2004.
5. A. Gilchrist, A. G. White, and W. J. Munro, "Entanglement creation using quantum interrogation," *Physical Review A* **66**(1), p. 012106, 2002.
6. A. G. White, J. R. Mitchell, O. Nairz, and P. G. Kwiat, "'Interaction-free' imaging," *Physical Review A* **58**(1), pp. 605–613, 1998.
7. C. Brukner and A. Zeilinger, "Young's experiment and the finiteness of information," *Philosophical Transactions of the Royal Society of London Series A-Mathematical Physical and Engineering Sciences* **360**(1794), pp. 1061–1069, 2002.
8. A. Gilchrist, K. Nemoto, W. J. Munro, T. C. Ralph, S. Glancy, S. L. Braunstein, and G. J. Milburn, "Schrödinger cats and their power for quantum information processing," *Journal of Optics B-Quantum and Semiclassical Optics* **6**(8), pp. S828–S833, 2004.
9. D. K. L. Oi, "Interference of quantum channels," *Physical Review Letters* **91**(6), p. 067902, 2003.
10. A. Luis, "Operational approach to complementarity and duality relations," *Physical Review A* **70**(6), p. 62107, 2004.
11. A. G. White, D. F. V. James, W. J. Munro, and P. G. Kwiat, "Exploring Hilbert space: Accurate characterization of quantum information," *Physical Review A* **65**(1), p. 012301, 2002.
12. A. I. Lvovsky and T. Aichele, "Conditionally prepared photon and quantum imaging," in *Quantum Communications and Quantum Imaging II*, R. E. Meyers and Y. Shih, eds., **5551**, pp. 1–6, SPIE, (Denver, CO, USA), 2004.

13. R. P. Feynman, *QED: the strange theory of light and matter*, Alix G. Mautner memorial lectures, Princeton University Press, Princeton, N.J., 1985.
14. R. P. Feynman, *Quantum electrodynamics; a lecture note and reprint volume*, W.A. Benjamin, New York, 1961.
15. R. P. Feynman and A. R. Hibbs, *Quantum mechanics and path integrals*, International series in pure and applied physics, McGraw-Hill, New York, 1965.
16. E. F. Taylor, S. Vokos, J. M. O'Meara, and N. S. Thornber, "Teaching Feynman's sum-over-paths quantum theory," *Computers in Physics* **12**(2), pp. 190–199, 1998.
17. C. Mead and L. Conway, *Introduction to VLSI systems*, Addison-Wesley, Reading, Mass., 1980.
18. C. Niclass, A. Rochas, P. A. Besse, and E. Charbon, "Toward a 3-d camera based on single photon avalanche diodes," *IEEE Journal of Selected Topics in Quantum Electronics* **10**(4), pp. 796–802, 2004.
19. S. S. Afshar, "Sharp complementarity wave and particle behaviours in the same welcher Weg experiment." <http://irims.org/quant-ph/030503/index.htm>, October 2004.
20. R. P. Feynman, *Statistical mechanics; a set of lectures*, Frontiers in physics, W. A. Benjamin, Reading, Mass., 1972.
21. N. J. Gunther and T. Kalotas, "Comment on the classical limit of Feynman path integrals," *American Journal of Physics* **45**(10), p. 1000, 1977.
22. E. P. Storey and C. Cohen-Tannoudji, "The Feynman path-integral approach to atomic interferometry - A tutorial," *Journal De Physique II* **4**(11), pp. 1999–2027, 1994.
23. A. Peters, K. Y. Chung, B. Young, J. Hensley, and S. Chu, "Precision atom interferometry," *Philosophical Transactions of the Royal Society of London Series A-Mathematical Physical and Engineering Sciences* **355**(1733), pp. 2223–2233, 1997.
24. A. Einstein, "Quantentheorie der Strahlung," *Physikalische Zeitschrift* **18**, pp. 121–128, 1917.
25. N. Bohr, "Discussion with Einstein on epistemological problems in atomic physics," in *Albert Einstein: Philosopher-Scientist*, P. Schlipp, ed., **1**, pp. 201–241, Harper, New York, 1949.
26. M. Born and E. Wolf, *Principles of optics; electromagnetic theory of propagation, interference and diffraction of light*, Pergamon Press, Oxford, New York, 4th ed., 1970.
27. E. J. Galvez, C. H. Holbrow, M. J. Pysher, J. W. Martin, N. Courtemanche, L. Heilig, and J. Spencer, "Interference with correlated photons: Five quantum mechanics experiments for undergraduates," *American Journal of Physics* **73**(2), pp. 127–140, 2005.
28. P. A. M. Dirac, *The Principles of Quantum Mechanics*, International series of monographs on physics, Clarendon Press, Oxford, 4th ed., 1958.
29. C. H. Holbrow, E. Galvez, and M. E. Parks, "Photon quantum mechanics and beam splitters," *American Journal of Physics* **70**(3), pp. 260–265, 2002.
30. D. N. Klyshko, "Effect of focusing on photon-correlation in parametric scattering of light," *Zhurnal Eksperimentalnoi I Teoreticheskoi Fiziki* **94**(6), pp. 82–90, 1988. Sov. Phys. JETP, 87, 6, 1131–1135, June 1988.
31. D. N. Klyshko, "A simple method of preparing pure states of the optical-field, a realization of the Einstein, Podolsky, Rosen experiment and a demonstration of the complementarity principle," *Uspekhi Fizicheskikh Nauk* **154**(1), pp. 133–152, 1988. Sov. Phys. Usp. 31, 1, 74–85, January 1988.
32. D. N. Klyshko, "Quantum optics: Quantum, classical, and metaphysical aspects," in *Fundamental problems in quantum theory: a conference held in honor of professor John Archibald Wheeler*, D. M. Greenberger and A. Zeilinger, eds., *Annals of the New York Academy of Sciences* **755**, pp. 13–27, The New York Academy of Sciences, New York, 1995.
33. J. A. Wheeler and R. P. Feynman, "Interaction with the absorber as the mechanism of radiation," *Reviews of Modern Physics* **17**, pp. 157–181, 1945.
34. T. Gold and H. Bondi, *The nature of time*, Cornell University Press, Ithaca, N.Y., 1967.
35. J. G. Cramer, "The transactional interpretation of quantum-mechanics," *Reviews of Modern Physics* **58**(3), pp. 647–687, 1986.
36. M. Chown, "Quantum rebel," *New Scientist* **183**(2457), pp. 30–35, 2004.
37. W. Unruh, "Shahriar Afshar: Quantum rebel?." <http://axion.physics.ubc.ca/rebel.html>, August 2004.

38. P. Epinasse, “Bohr’s complementarity principle challenged after 80 years,” *OE Magazine* **5**, p. 8, January 2005.
39. S. S. Afshar, “Response to W. Unruh.” <http://users.rowan.edu/~afshar/FAQ.htm>, August 2004.
40. N. J. Gunther, “Afshar explained.” <http://www.neilgunther.com/Photonz/Afshar/AfsharX0305.pdf>, March 2005.
41. P. D. D. Schwindt, P. G. Kwiat, and B.-G. Englert, “Quantitative wave-particle duality and nonerasing quantum erasure,” *Physical Review A* **60**(6), pp. 4285–4290, 1999.
42. G. Brida, A. Genovese, A. Gramegna, and E. Predazzi, “A conclusive experiment to throw more light on ‘light’,” *Physics Letters A* **328**(4-5), pp. 313–318, 2004.
43. A. Bramon, R. Escribano, and G. Garbarino, “Bell’s inequality tests: from photons to B-mesons.” <http://arxiv.org/abs/quant-ph/0410122>, 2004.
44. J. A. Wheeler, “The ‘past’ and the ‘delayed-choice’ double-slit experiment,” in *Mathematical Foundations of Quantum Theory*, A. Marlow, ed., pp. 9–48, Academic Press, New York, 1978.
45. W. K. Wootters and W. H. Zurek, “Complementarity in the double-slit experiment: Quantum nonseparability and a quantitative statement of Bohr’s principle,” *Physical Review D* **19**(2), pp. 473–484, 1979.
46. L. Bartell, “Complementarity in the double-slit experiment: On simple realizable systems for observing intermediate particle-wave behavior,” *Physical Review D* **21**(6), pp. 1698–1699, 1980.
47. C. S. Wu and I. Shaknov, “The angular correlation of scattered annihilation radiation,” *Physical Review* **77**, pp. 136–136, 1950.
48. H. Zbinden, J. Brendel, N. Gisin, and W. Tittel, “Experimental test of nonlocal quantum correlation in relativistic configurations,” *Physical Review A* **63**(2), p. 022111, 2001.
49. E. F. Taylor and D. Styer, “cT executor program, version 3.” <http://www.eftaylor.com/download.html#quantum>, 2000.
50. M. Harowitz, H. Shin, and J. Shumway, “Path-integral quantum Monte Carlo techniques for self-assembled quantum dots,” *Journal of Low Temperature Physics* **Submitted**, 2005.